

Structural properties and cyclic oxidation behavior of Ni-Al-Y superalloys

Mehmet Sahin Atas, Mehmet Yildirim*

*Konya Technical University, Faculty of Engineering and Natural Sciences,
Department of Metallurgical and Materials Engineering, Konya, Turkey*

Received 24 December 2021, received in revised form 26 August 2022, accepted 5 September 2022

Abstract

The microstructure, microhardness, and oxidation resistance of ternary model Ni-13Al-2Y (at.%) and Ni-11Al-4Y (at.%) superalloys were studied in detail. The microstructures of alloys consisted of primary γ -Ni dendrites and residual eutectic. The Ni_{17}Y_2 intermetallic and γ -Ni were the major constituents of the eutectic phase mixture. The microhardness value of Ni-11Al-4Y alloy was higher than that of Ni-13Al-2Y alloy because of the higher amount of relatively harder eutectic. With increasing Y concentration from 2 to 4 at.%, the mass gain, oxide scale thickness, and oxidation rate remarkably increased. For both alloys, the oxide scale was comprised of three layers: NiO as a surface layer, Al_2O_3 as an inner layer in the metal/oxide interface, and mixed Al/Y oxides as an internal layer. Although the studied alloys exhibited fairly good scale adherence in conjunction with almost no important scale spallation, they exhibited faster oxidation kinetics along with higher mass gains.

Key words: Ni-based superalloys, microstructure, cyclic oxidation, kinetics

1. Introduction

Ni-based superalloys are key materials for high-temperature applications such as blades, nozzle guide vanes, and discs in aircraft engines and industrial steam turbines, owing to their high-temperature strength, creep resistance, and satisfactory corrosion/oxidation resistance [1–8]. In these applications, components typically experience high stresses under oxidative atmosphere [9]. Thus, oxidation resistance of Ni-based superalloys is one of the crucial service life determining factors of the components [10–12]. The efficiency of aero engines and land-based gas turbines could be significantly enhanced by increasing the operating temperatures. As the service temperature increases, rapid degradation of superalloys inevitably occurs [3, 9, 10, 13–18]. Therefore, the design and development of novel Ni-based superalloys with better mechanical properties and oxidation resistance are needed [19].

Oxidation behavior of superalloys depends on several factors such as the composition of the alloy (i.e., Al and Cr concentration, type and content of alloying

elements), gas atmosphere, surface condition, cracking, and spallation behavior of the oxide scale [10, 13, 20–23]. When a bare Ni-based superalloy is exposed to an oxygen-rich atmosphere, the formation of oxide particles on its surfaces arises, and then they coalesce quickly to develop a continuous layer as the oxidation process continues [10]. A dense, continuous, adherent, thermodynamically stable, protective, and slowly growing oxide layer must be formed to prevent the degradation of superalloy [24]. Cr_2O_3 and α - Al_2O_3 could be accounted as the most protective oxides. Compared to Cr_2O_3 forming superalloys, Al_2O_3 is the one exhibiting higher oxidation resistance for two main reasons: (i) low diffusion rate through Al_2O_3 scales and (ii) transformation of Cr_2O_3 to volatile CrO_3 at high temperatures ($> 900^\circ\text{C}$) [3, 24–28]. Thus, Al_2O_3 is mostly preferred commercial superalloy as a component due to operating temperatures higher than 1000°C [3, 29].

The properties of oxide layers, such as adherence and scale spallation resistance, gain importance for metallic substrates along with slow oxidation kinetics and oxidation product, especially under thermal cy-

*Corresponding author: tel.: +90 332 2051933; e-mail address: mvildirim@ktun.edu.tr

cling circumstances [3]. It is well-known that the scale spallation resistance of superalloys can be improved by adding a minor amount of reactive elements such as Y, Ce, La, Zr, or Hf [3, 30–35]. Among these elements, Y positively affects the mechanical properties and oxidation resistance of Ni-based superalloys and is considered a potential alloying element.

The effect of a minor amount (typically less than 0.5 wt.%) of Y addition on the microstructure, mechanical properties, and oxidation behavior of Ni-based superalloys and some alumina-forming alloys is investigated in a series of experimental studies [30, 32–38]. These studies reported that a minor amount of Y addition reduced the oxidation rate and enhanced the inherent strength of the superalloy/oxide interface. However, Pint et al. [33–35] presented that a high amount of Y addition may lead to extensive internal oxidation in conjunction with considerably increased oxidation rates. They also reported that a very small amount of Y addition into alumina forming alloys such as FeCrAl and NiCoCrAl improves the alumina scale adherence, but the alloys with high Y concentration would be expected to the scale spallation. Although there are hypotheses to predict the oxidation behavior of alloys with high Y contents, the experimental data is still missing. Therefore, in this present study, the microstructures, microhardness, and the cyclic oxidation behavior of ternary model Ni-13Al-2Y and Ni-11Al-4Y (hereafter compositions will be referred to as at.%) superalloys were examined in depth.

2. Experimental procedure

2.1. Sample production

The Ni-13Al-2Y and Ni-11Al-4Y alloy ingots weighing 25 g were manufactured by vacuum arc-melting under an argon atmosphere. Appropriate amounts of ultrahigh purity elements (> 99.90%) were used during melting. The alloy ingots were re-melted three times to obtain compositional homogeneity. Then, the arc-melted ingots were subjected to three-step heat treatment: (i) homogenization at 1250 °C for 24 h, (ii) solutionizing in the single phase γ region (above the solidus temperature) at 1150 °C for 3 h, followed by ice-water quenching to hinder γ' formation, and (iii) aging at 800 °C for 1, 4, 16, 64, and 256 h. All heat treatments were performed with a muffle furnace under laboratory air.

2.2. Characterization

The microstructural examination of the specimens was conducted utilizing a Hitachi SU5000 model field-emission-gun scanning electron microscope (FEG-SEM). Before SEM analysis, specimens were ground

using emery papers (320 to 1200 grit) and polished with an alumina suspension of 1 μm particles. The solution of 100 mL HCl, 100 mL deionized H_2O , and 1 g $\text{K}_2\text{S}_2\text{O}_5$ was used as an etchant. The chemical composition of the alloys and the constituent phases were measured by utilizing an energy dispersive spectrometer (EDS) attached to an SEM. The phase analysis of the specimens was done by X-ray diffraction (XRD) analysis on a Bruker D8 system with Cu-K α radiation, indexed in the 2θ range of 30°–100°. The lattice parameters of the phases were calculated with the well-known Bragg's law. The Vickers microhardness values of specimens were determined using a Microbul 1000D microhardness test equipment at 200 g load and a dwelling time of 10 s. At least ten independent indentations were taken on each specimen to get an average microhardness value.

2.3. Cyclic oxidation tests

Specimens for the cyclic oxidation experiments were machined from the ingots with the dimensions of 20 mm \times 8 mm \times 2 mm. For each composition, one specimen was utilized for the oxidation tests. Before testing, the specimens were abraded with emery papers (up to 1200 grit) and polished with 1 μm alumina suspension. Then, the specimens were ultrasonically cleaned in ethanol, dried in the air, and weighed. The specimen was placed in pure alumina crucibles. Cyclic oxidation tests were carried out using a muffle furnace preset at 1000 °C in air. After isothermal oxidation at 1000 °C for 1 h, the specimens were rapidly cooled to room temperature, and the weight changes of the specimens were measured simultaneously using an electronic balance (with an accuracy of 0.01 mg). The imaging of the oxidation products was conducted by utilizing SEM in back-scattered electron (BSE) and secondary electron (SE) modes. Cross-sectional EDS mapping and point scans were used to determine the chemical composition of the oxides.

3. Results and discussion

3.1. Microstructural evolution

The solidification microstructures of the as-cast Ni-13Al-2Y and Ni-11Al-4Y superalloys are shown in Fig. 1. The composition of the constituent phases present in the microstructures was identified by EDS (Table 1) and XRD (Fig. 2) analyses. The microstructures of as-cast Ni-Al-Y superalloys consisted of γ (Ni) primary dendrites, interdendritic zones composed of fine eutectic Ni_{17}Y_2 lamellas embedded in γ (Ni) matrix, and Ni_5Y particles formed close to the primary dendrites. The amount of the eutectic phase was increased with increasing Y content. Based on the EDS

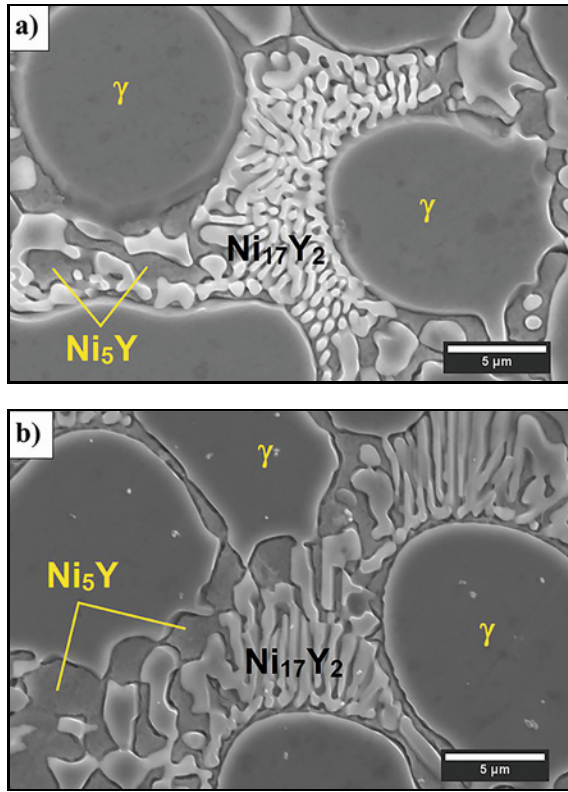


Fig. 1. SEM micrographs of as-cast (a) Ni-13Al-2Y and (b) Ni-11Al-4Y alloys.

analysis, Y solubility of the γ (Ni) phase was determined as 0.4 at.%. Beaudry and Daane [39] determined the Y solubility of the γ (Ni) phase as nearly 0.2 at.%. The calculated lattice parameter of the FCC γ (Ni) phase also verified the restricted solid solubility of Y in the γ (Ni) phase. The lattice parameters of the FCC γ (Ni) phase for Ni-13Al-2Y and Ni-11Al-4Y superalloys were calculated as 3.557 and 3.569 Å, respectively. The lattice parameter of the FCC γ (Ni) phase for Ni-Al based superalloys is known as 3.55 Å [40]. The dissolution of Y atoms, having a relatively higher atomic radius ($r_Y = 1.80$ Å) compared to Ni ($r_{Ni} = 1.245$ Å) and Al ($r_{Al} = 1.25$ Å) atoms, in the FCC γ (Ni) phase leads to an increment in lattice parameter.

With the increasing presence of Y from 2 to 4 at.%, the morphology and the size of the constituent phases did not apparently change, while the volume fraction of the eutectic mixture increased. However, the microstructures of the studied compositions highly changed after heat treatment (Figs. 3 and 4). The Ni₅Y intermetallic disappeared where the fine eutectic Ni₁₇Y₂ lamellas spheroidized and transformed into particles distributed along the grain boundaries of γ (Ni) dendrites. The coarsening and spheroidization of Ni₁₇Y₂ after aging can be explained by the Gibbs-Thomson effect [41, 42]. During solidification,

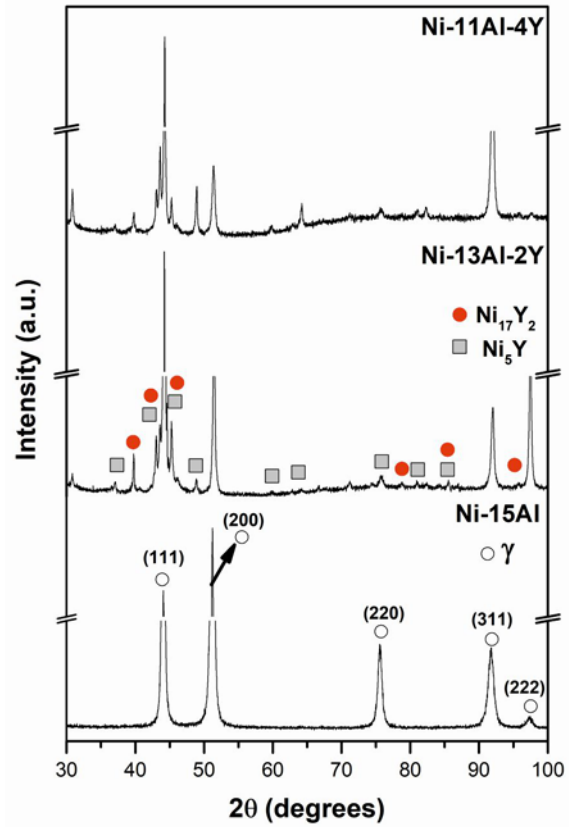


Fig. 2. XRD diffraction patterns of as-cast Ni-13Al-2Y and Ni-11Al-4Y alloys (the diffraction pattern of Y-free binary Ni-15Al was provided as a comparison).

Table 1. EDS analysis of the constituent phases present in the microstructures of as-cast Ni-13Al-2Y and Ni-11Al-4Y superalloys

		Ni-13Al-2Y		Ni-11Al-4Y	
		(wt.%)	(at.%)	(wt.%)	(at.%)
γ (Ni)	Ni	93.8	87.9	93.3	87.1
	Al	5.8	11.8	6.2	12.6
	Y	0.4	0.3	0.5	0.3
Ni ₁₇ Y ₂	Ni	85.4	88.4	86.4	89.0
	Al	1.1	2.3	1.1	2.5
	Y	13.5	9.3	12.5	8.5
Ni ₅ Y	Ni	77.1	80.4	77.1	80.2
	Al	2.4	5.5	2.6	5.8
	Y	20.5	14.1	20.3	14.0

the growth of eutectic is accelerated by the lateral diffusion of solutes in the solid/liquid interface. Moreover, the fine lamellar eutectic possesses more interfacial energy, which is the driving force in this mate-

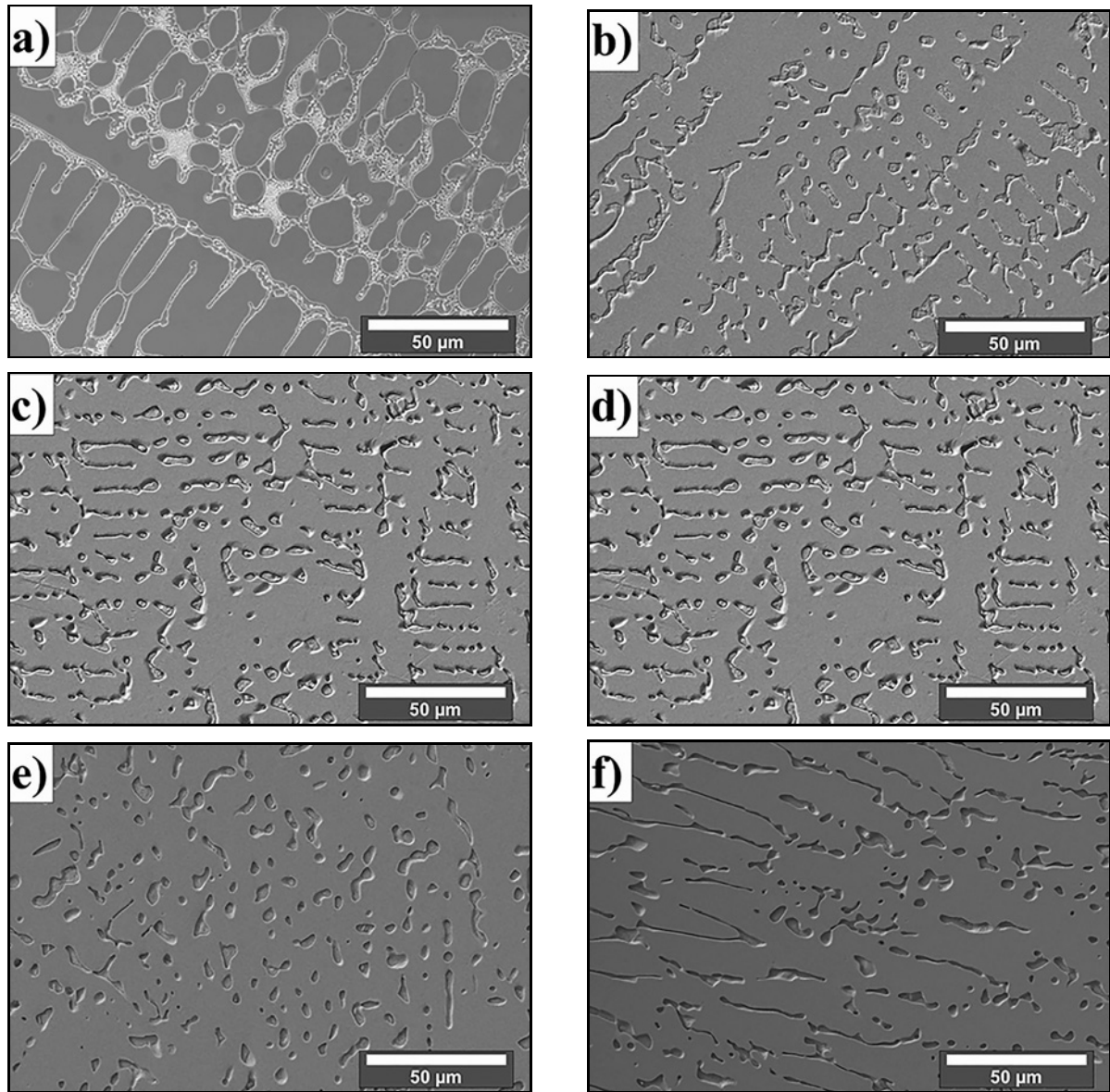


Fig. 3. SEM micrographs of studied Ni-13Al-2Y alloys: (a) as-cast, (b) 1 h, (c) 4 h, (d) 16 h, (e) 64 h, and (f) 256 h aged.

Table 2. Microhardness values of as-cast and 0 h aged Ni-13Al-2Y and Ni-11Al-4Y superalloys

Alloys (at.%)	Microhardness (GPa)	
	As-cast	0 h
Ni-13Al-2Y	2.9 ± 0.1	2.2 ± 0.1
Ni-11Al-4Y	3.3 ± 0.2	2.7 ± 0.2

rial system. The eutectic/dendrite interface acts as a heterogeneous region for the interaction of Ni and Y during annealing. As the interfacial energy decreases, the lamellar eutectic tends to fragment and transform into spherical particles [42, 43].

The microstructural alterations after aging strong-

ly influenced the microhardness values of Ni-13Al-2Y and Ni-11Al-4Y superalloys (Fig. 5). Among the investigated specimens, as-cast superalloys (Table 2) exhibited higher microhardness values compared to aged ones. It was observed that the microhardness value of both triple Ni-Al-Y casting samples was relatively high. The highest microhardness values of 2.9 GPa and 3.3 GPa were obtained in the casting samples of Ni-13Al-2Y and Ni-11Al-4Y superalloys, respectively. The spherodization and coarsening of fine lamellas led to a considerable decrease in hardness. Traditionally, the microhardness values of Ni-based superalloys enhance after aging and exhibit a peak (maximum) hardness nearly at 4 h aging time [6, 11, 12, 44–46]. In the present study, the mean microhardness values drastically decreased after aging due to

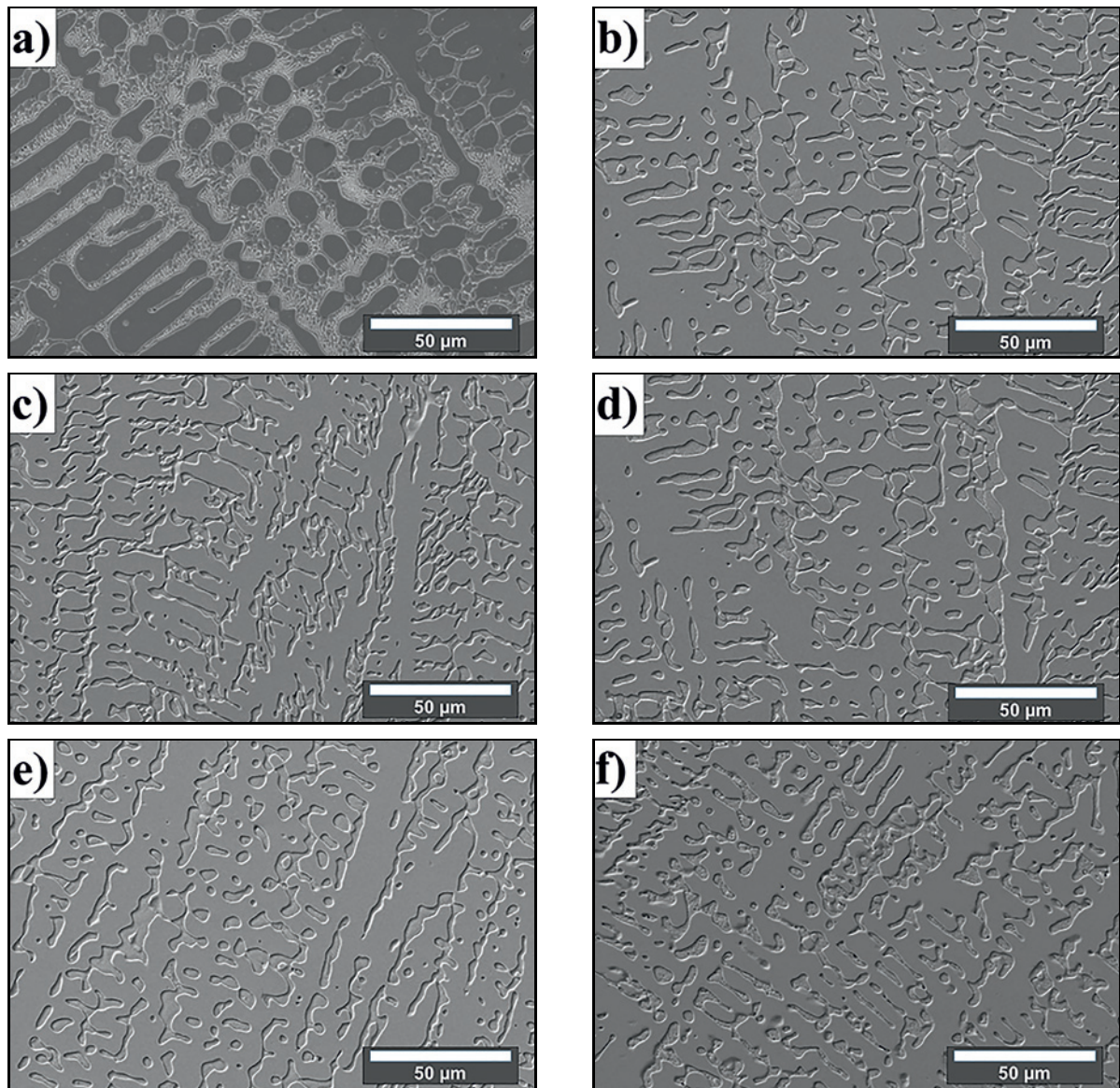


Fig. 4. SEM micrographs of studied Ni-11Al-4Y alloys: (a) as-cast, (b) 1 h, (c) 4 h, (d) 16 h, (e) 64 h, and (f) 256 h aged.

spheroidization and coarsening of fine Ni_{17}Y_2 lamellas. The microhardness values of Ni-11Al-4Y superalloys were 1.1–1.35 times greater than those of Ni-13Al-2Y superalloys since the amount of hard Ni_{17}Y_2 intermetallic is higher for Ni-11Al-4Y composition. Compared to the microhardness profile of Y-free binary Ni-15Al superalloy studied in our previous study [11], the as-cast Ni-Al-Y alloys were considerably harder. However, in the present study, the formation of the γ' -(Ni_3Al) phase was observed in neither as-cast nor aged specimens. Y has an incomplete solid solubility in γ -Ni and Ni_5Y and/or Ni_{17}Y_2 phases, which can be formed even at a minor amount of Y addition [39, 47, 48]. Based on the results of the point EDS analyses, γ -Ni has an important Al solid solubility, which was determined as nearly 12.5 at.%. In addition, Al has an obvious solid solubility in Ni_5Y

and Ni_{17}Y_2 phases. The point EDS analysis (Table 1) also revealed that the Al concentrations of Ni_5Y or Ni_{17}Y_2 are found to be nearly 5.5 and 2.5 %, respectively. According to these results, Ni_5Y and Ni_{17}Y_2 phases behave as Ni_5Y - or Ni_{17}Y_2 -based solid solutions instead of binary intermetallics. Wu et al. [47, 48] studied the Ni-Al-Y system, and similar outcomes supporting our findings were acquired. They also observed that γ' -(Ni_3Al) did not form in the microstructures of Ni-10Al-3Y and Ni-10Al-10Y alloys. Moreover, they also reported that the Ni_5Y phase has an Al concentration of 4.6 and 6.4 at.% for Ni-10Al-3Y and Ni-10Al-10Y compositions, respectively. Thus, it can be concluded that a high amount of Al is consumed by γ -Ni, Ni_5Y , and Ni_{17}Y_2 phases in the microstructure, which suppressed the formation of the γ' -(Ni_3Al) phase.

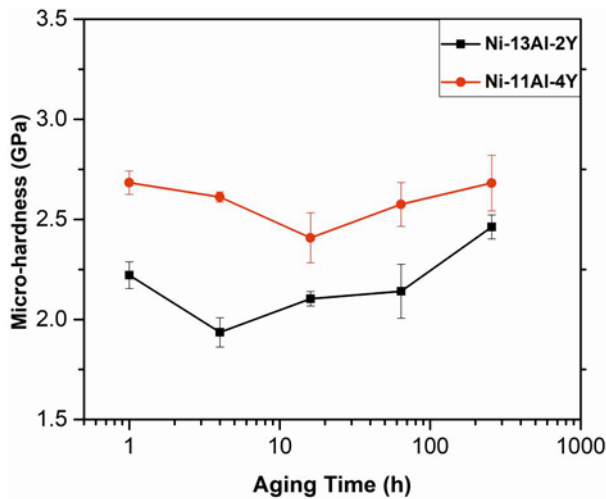


Fig. 5. The Vickers microhardness profile of the studied Ni-Al-Y alloys.

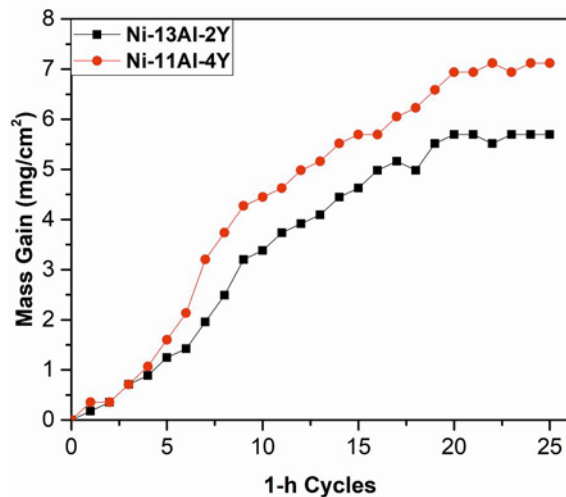


Fig. 6. Kinetic plots of the Ni-Al-Y alloys oxidized at 1000°C in air.

3.2. Oxidation behavior

The oxidation kinetics plots of Ni-Al-Y alloys at 1000°C in the air are displayed in Fig. 6. Because of the degeneration of the eutectic and strong reduction in the microhardness values after isothermal aging, we have investigated the oxidation behavior of only as-cast Ni-Al-Y alloys in detail. The mass gain of both alloys increased with time up to the 20th cycle and then almost reached a plateau. It is clear that mass gain increased with increasing Y concentration. No significant scale spallation was observed in the mass gain vs. time plots of the studied Ni-Al-Y alloys. The oxidation process almost obeyed the parabolic rate law for the studied temperature of 1000°C.

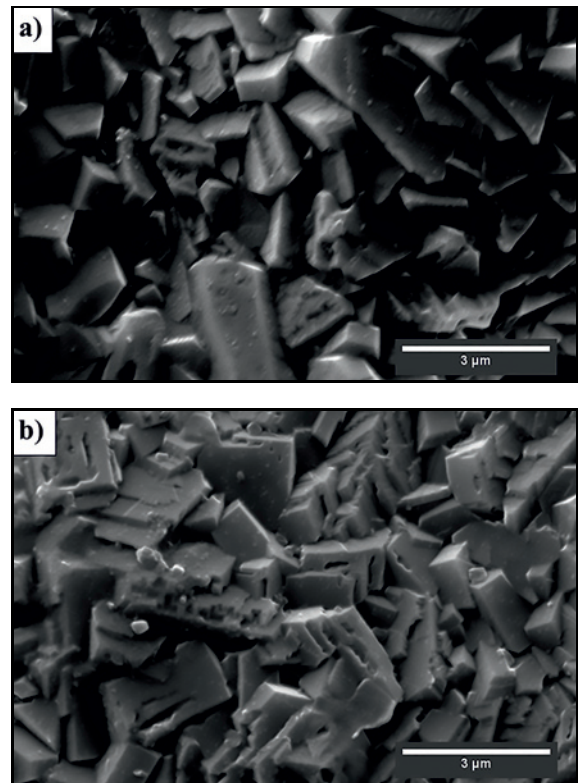


Fig. 7. Surface scale morphology of the oxidized specimens: (a) Ni-13Al-2Y and (b) Ni-11Al-4Y alloys.

Several pure metals and engineering alloys follow parabolic kinetics at high temperatures. Parabolic oxidation occurs when the metal or oxygen ions transport to the growing oxide scale [49]. According to this law, as the oxide scale thickness increases, the diffusion of these ions decreases, which reduces the oxidation rate. The values of parabolic rate constants (k_p) were determined utilizing the parabolic rate equation given by:

$$\left(\frac{\Delta W}{A}\right)^2 = k_p t, \quad (1)$$

where $\left(\frac{\Delta W}{A}\right)$ is the mass gain per unit surface area (mg cm^{-2}), k_p is the parabolic rate constant ($\text{mg}^2 \text{cm}^{-4} \text{s}^{-1}$), and t is the oxidation time (s). The parabolic rate constants for the Ni-13Al-2Y and Ni-11Al-4Y alloys were determined as $4.5 \times 10^{-4} \pm 1.8 \times 10^{-5}$ and $6.7 \times 10^{-4} \pm 2.0 \times 10^{-5} \text{ mg}^2 \text{cm}^{-4} \text{s}^{-1}$, respectively. The parabolic rate constant for Ni-11Al-4Y alloy was relatively higher than that of Ni-13Al-2Y alloy since the weight gain for Ni-11Al-4Y alloy was reasonably higher. The calculated k_p values for Ni-Al-Y alloys were compared to the k_p value of Y-free binary Ni-15Al studied in our previous study [11]. The substantially lower k_p value ($2.99 \times 10^{-5} \pm 1.81 \times 10^{-6} \text{ mg}^2 \text{cm}^{-4} \text{s}^{-1}$) of Ni-15Al

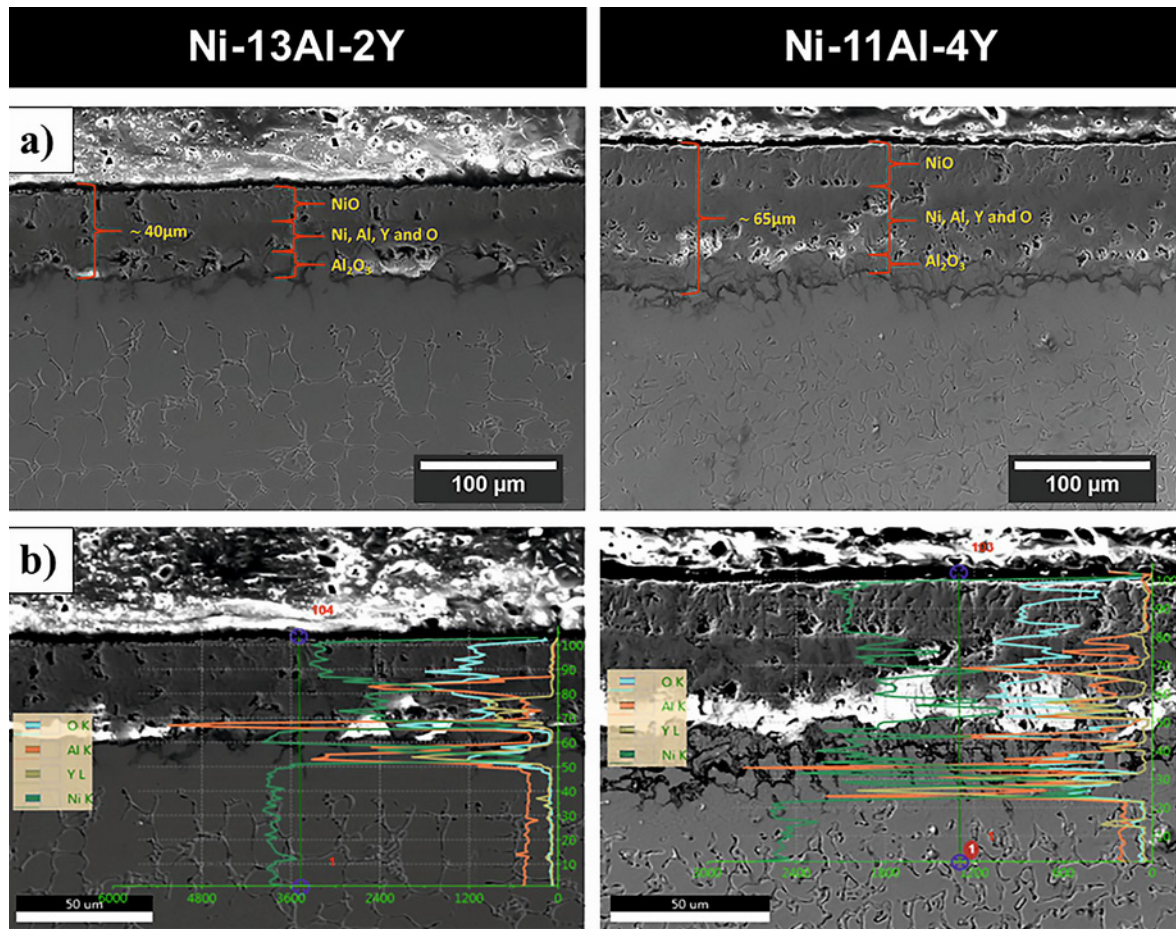


Fig. 8. (a) Cross-section images of oxide scales formed on the specimens of Ni-13Al-2Y and Ni-11Al-4Y alloys and (b) the linear elemental distributions of oxide scales in SEM-BSE mode.

strongly indicated the faster oxidation kinetics in the presence of Y.

The morphologies of the surface scales for Ni-Al-Y alloys are shown in Fig. 7. The surface scale was compact, dense, adherent, and uniformly distributed for both alloys. The scale morphologies of both alloys were composed of typical blocky and coarse NiO oxides. In addition, any defects such as cracks or cavities were not observed in the surface scales. However, examining surface scales does not reflect the whole high-temperature oxidation process. Internal oxides can be formed beneath the surface scale. Thus, cross-sectional SEM-EDS (Fig. 8) and elemental mapping analyses (Figs. 9 and 10) were performed.

According to these analyses, the oxide scale consisted of three layers: (i) dense NiO surface layer with a thickness of approximately 12 and 21 μm for Ni-13Al-2Y and Ni-11Al-4Y alloys, respectively. (ii) The middle layer was composed of oxides containing Ni, Al, and Y. The chemical compositions of the oxides present in the middle layer could not be determined quantitatively by EDS analysis. However, the qualitative EDS measurements showed that this layer might be composed of mixed Al/Y oxides. The thicknesses of

this layer were measured as 17 and 29 μm for Ni-13Al-2Y and Ni-11Al-4Y alloys, respectively. (iii) The thin and continuous inner layer in the metal/oxide interface was mainly constituted of Al_2O_3 . The formation of the thin Al_2O_3 layer in the metal/oxide interface was also confirmed by the EDS point analysis given in Fig. 11.

Ni-based alloys are classified into three main groups concerning the oxides forming on the surfaces: (a) alumina (Al_2O_3) formers, (b) chromia (Cr_2O_3) formers, and (NiO) formers. Among these alloys, alumina formers show better oxidation resistance at high temperatures. Protective chromia scales transform into non-protective Cr_2O_3 scale above 900 $^\circ\text{C}$. If the concentration of Al or Cr is sufficient, protective Al_2O_3 and Cr_2O_3 external scales are developed. In the present study, the predominant NiO external scale was formed since the concentration of Al was relatively low. In the early cycles of oxidation, continuous and dense NiO scales were quickly formed to produce an external scale. On the other hand, the thin Al_2O_3 internal scale was only developed at the alloy/oxide interface via internal oxidation of Al because of the high affinity of aluminum

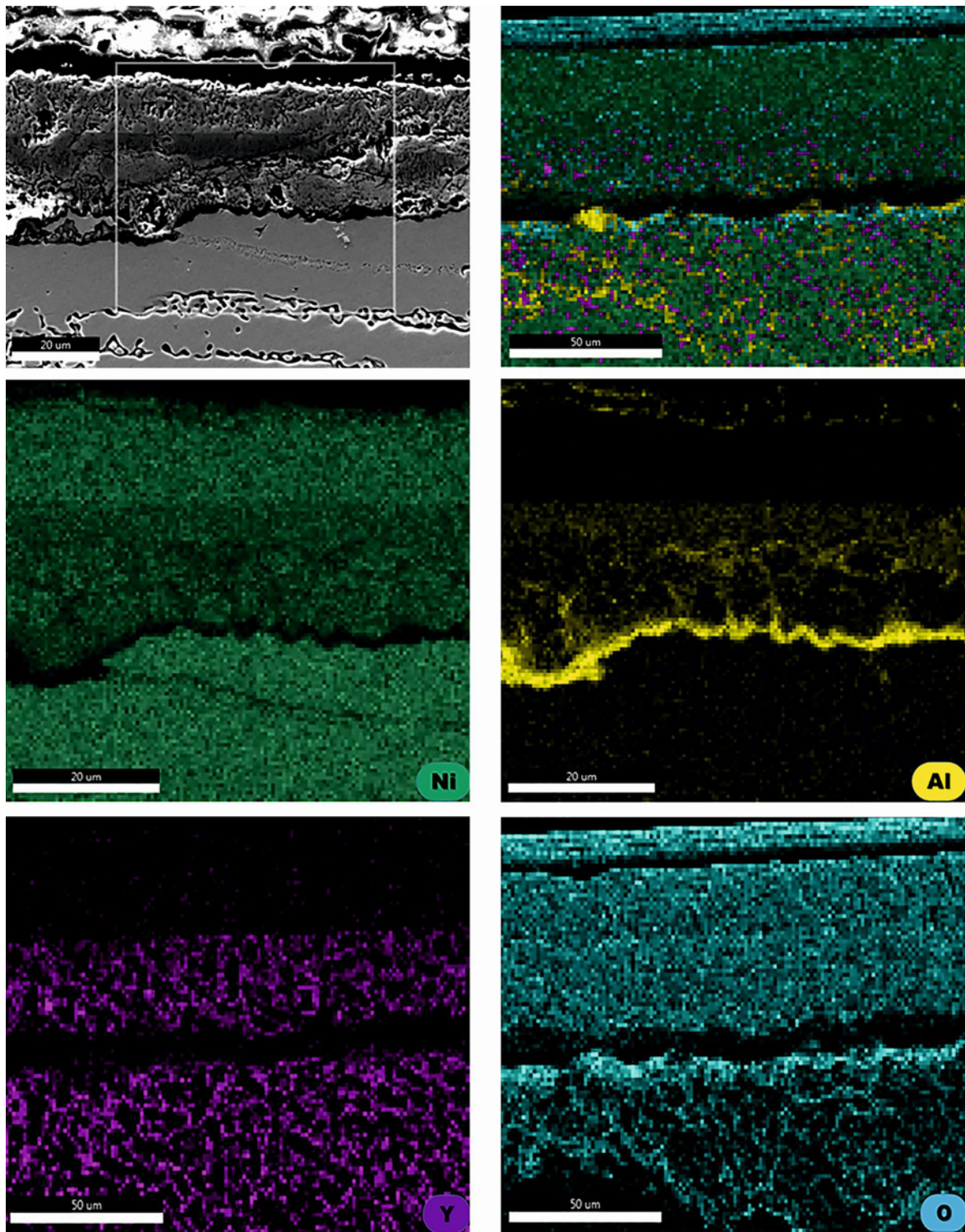


Fig. 9. SEM cross-section image and the corresponding EDS elemental mapping of the Ni-13Al-2Y specimen.

to oxygen. As the oxidation process proceeds, a continuous Al_2O_3 scale is formed [3]. In the intermediate layer, substantial internal oxidation of Y occurred, which led to significantly increased overall oxidation rates. Pint et al. [33–35] reported that Y frequently exists in the internal oxidation zone in

the form of mixed Al/Y oxides (e.g., garnets or perovskites).

In steady-state circumstances, various oxides can be present, and the oxidation product can be composed of different scales. The formation of an inner alumina scale inhibits the diffusion in the external di-

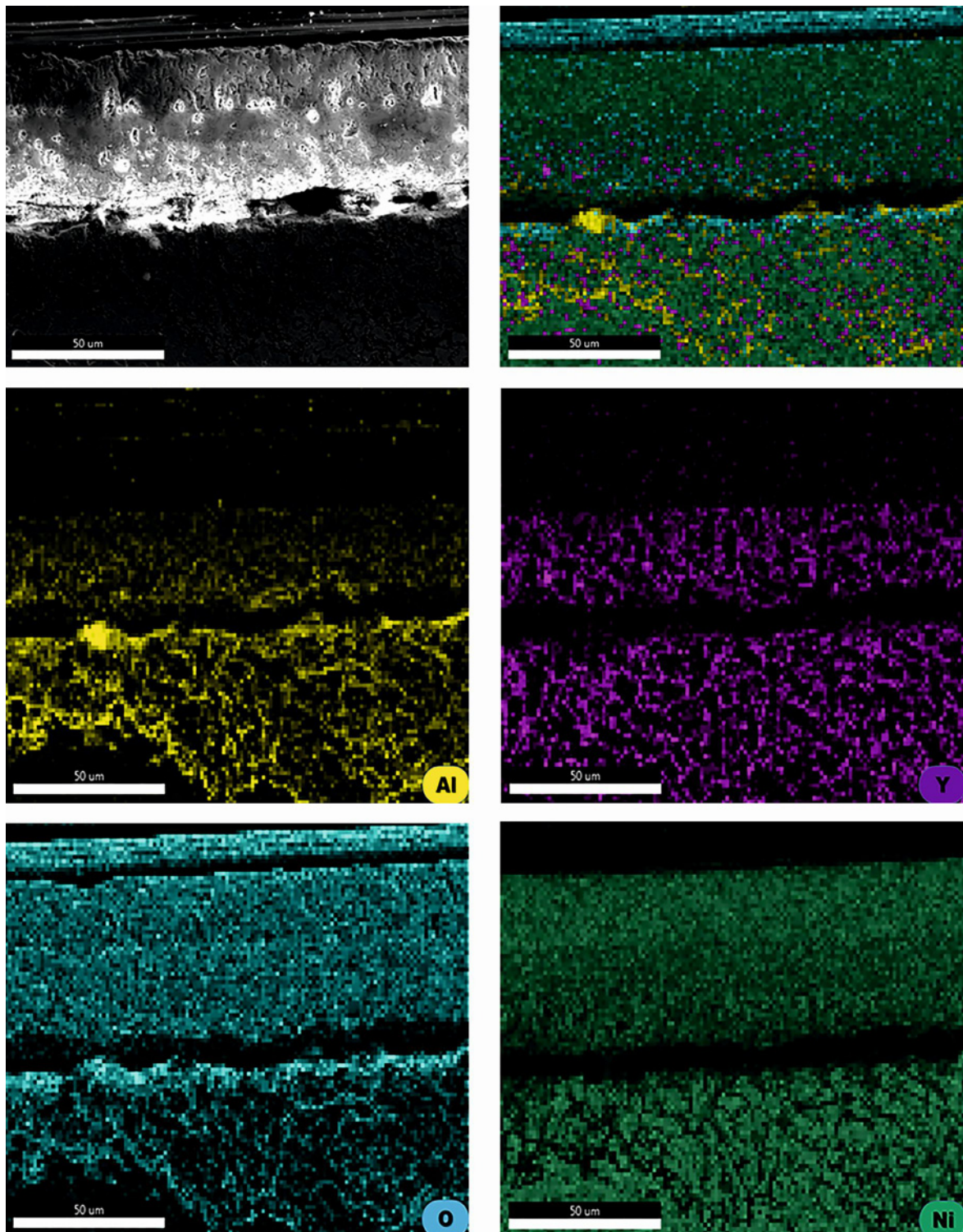


Fig. 10. SEM cross-section image and the corresponding EDS elemental mapping of the Ni-11Al-4Y specimen.

rection. Depending on the kinetics of inner alumina formation, the thickness of the scale can be various above the alumina layer, which causes a curved morphology of the metal/oxide interface [1]. In the present study, it can be concluded that the oxide scale thickness increased with increasing Y concentration.

Although the studied Ni-Al-Y alloys exhibited high oxidation rates due to the extensive internal oxidation, they exhibited fairly good scale adherence in conjunction with any significant scale spallation. The presence of Y, like other rare earth elements, plays a significant role in the release of the residual stresses formed dur-

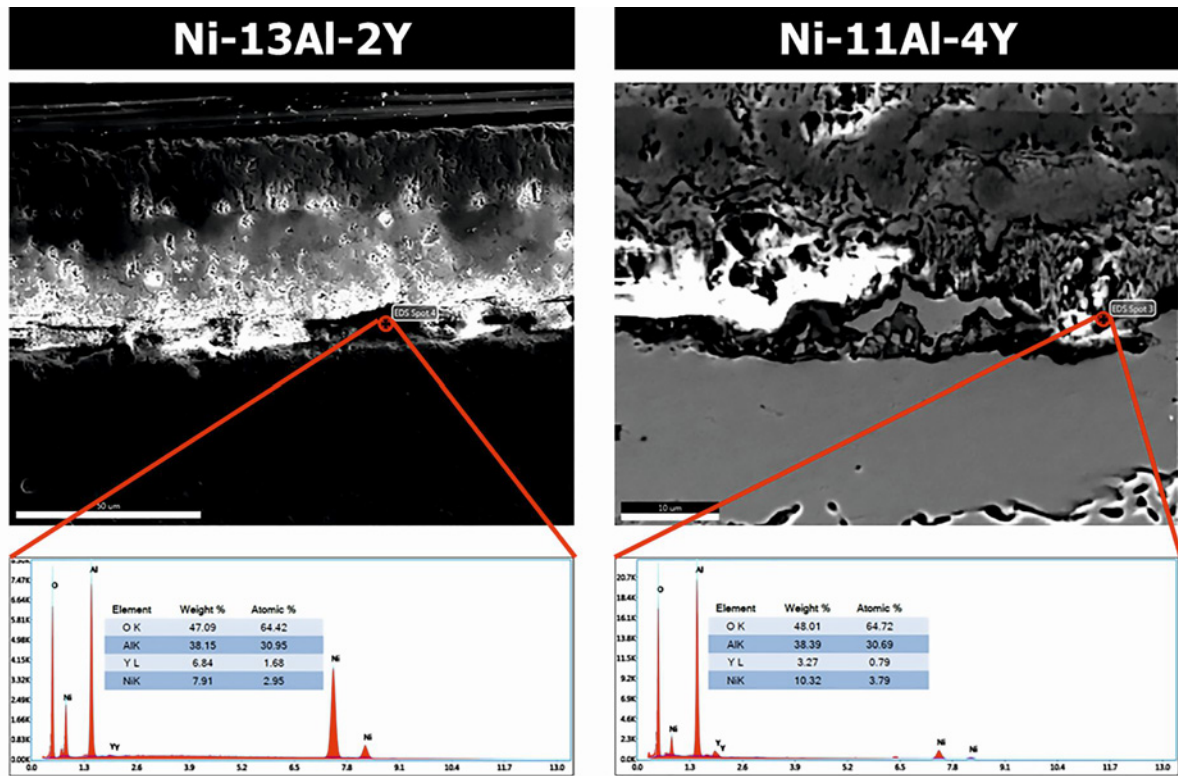


Fig. 11. SEM-EDS point analyses show the thin Al_2O_3 layer formation at the metal/oxide interface of Ni-13Al-2Y and Ni-11Al-4Y alloys.

ing thermal cycles [34, 35]. Therefore, alloys containing the Y element have good scale adherence, which is essential to the high-temperature oxidation behavior. Besides the good scale adherence with almost no defects such as cracks or pores, the formation of a non-protective NiO layer and the substantial internal oxidation zone restricted the development of outstanding oxidation resistance. To hinder the development of the internal oxidation zone, it is encouraged that Y concentration should be limited to low values (typically 0.1 wt.%).

The formation of the NiO scale as a surface oxide was directly ascribed to the insufficient Al concentrations of the studied alloys. According to the oxide diagram of Ni-Cr-Al based superalloys, NiO is the main oxidation product for alloys containing less than 10–11 wt.% Al [49]. Even though the Al concentrations of the present alloys are 13 and 11 at.%, the corresponding concentrations in wt.% are 6.4 and 5.3, respectively. Hence, the oxidation was controlled by the external diffusion of Ni ions, and the surface scale was composed of NiO.

It is suggested that the Al concentration should be increased to obtain outstanding oxidation resistance with superior surface scale morphology. The formation of Al_2O_3 as a surface scale would enhance the oxidation resistance.

4. Conclusions

The microstructure, microhardness, and cyclic oxidation behavior of Y-containing model Ni-Al based superalloys were examined. Based on the experimental results, the following conclusions can be summarized:

- The microstructures of the as-cast alloys were composed of primary γ -Ni dendrites and a eutectic mixture.
- The constituents of eutectic were determined as Ni_{17}Y_2 intermetallic and γ -Ni.
- After aging, Ni_{17}Y_2 fine lamellas strongly coarsened, reducing hardness.
- With increasing Y alloying element concentration, hardness substantially increased.
- Compared to Ni-13Al-2Y alloy, Ni-11Al-4Y alloy showed greater oxidation rates with relatively higher mass gains and increased oxide scale thickness.
- The oxide scales on both alloys consisted of three layers: (i) NiO as an external layer, (ii) an internal oxidation zone composed of Al/Y oxides, and (iii) alumina as an inner layer.

Acknowledgements

This study was partially supported by Konya Technical University OYP Program (2017-OYP-042). Special thanks

to Adem Sarılmaz and Mehmet Ali Topçu for the SEM-EDS analysis.

References

- [1] L. Klein, A. Bauer, S. Neumeier, M. Göken, S. Virtanen, High temperature oxidation of γ/γ' -strengthened Co-base superalloys, *Corrosion Science* 53 (2011) 2027–2034. <https://doi.org/10.1016/j.corsci.2011.02.033>
- [2] F. Weng, H. Yu, C. Chen, K. Wan, Fabrication of Ni-based superalloys containing Nb and their high temperature oxidation behaviors, *Materials and Manufacturing Processes* 30 (2015) 1364–1369. <https://doi.org/10.1080/10426914.2015.1037906>
- [3] Q. Feng, B. Tryon, L. Carroll, T. Pollock, Cyclic oxidation of Ru-containing single crystal superalloys at 1100°C, *Materials Science and Engineering A* 458 (2007) 184–194. <https://doi.org/10.1016/j.msea.2006.12.064>
- [4] T. M. Pollock, S. Tin, Nickel-based superalloys for advanced turbine engines: Chemistry, microstructure and properties, *Journal of Propulsion and Power* 22 (2006) 361–374. <https://doi.org/10.2514/1.18239>
- [5] F. H. Latief, K. Kakehi, Y. Tashiro, Oxidation behavior characteristics of an aluminized Ni-based single crystal superalloy CM186LC between 900 °C and 1100°C in air, *Journal of Industrial and Engineering Chemistry* 19 (2013) 1926–1932. <https://doi.org/10.1016/j.jiec.2013.02.039>
- [6] C. K. Sudbrack, T. D. Ziebell, R. D. Noebe, D. N. Seidman, Effects of a tungsten addition on the morphological evolution, spatial correlations and temporal evolution of a model Ni-Al-Cr superalloy, *Acta Materialia* 56 (2008) 448–463. <https://doi.org/10.1016/j.actamat.2007.09.042>
- [7] R. C. Reed, *The Superalloys: Fundamentals and Applications*, Cambridge University Press 2009. <https://doi.org/10.1017/CBO9780511541285>
- [8] K. E. Yoon, R. D. Noebe, D. N. Seidman, Effects of rhenium addition on the temporal evolution of the nanostructure and chemistry of a model Ni-Cr-Al superalloy. I: Experimental observations, *Acta Materialia* 55 (2007) 1145–1157. <https://doi.org/10.1016/j.actamat.2006.08.027>
- [9] S. Cruchley, H. Evans, M. Taylor, M. Hardy, S. Stekovic, Chromia layer growth on a Ni-based superalloy: Sub-parabolic kinetics and the role of titanium, *Corrosion Science* 75 (2013) 58–66. <https://doi.org/10.1016/j.corsci.2013.05.016>
- [10] D. Saber, I. S. Emam, R. Abdel-Karim, High temperature cyclic oxidation of Ni based superalloys at different temperatures in air, *Journal of Alloys and Compounds* 719 (2017) 133–141. <https://doi.org/10.1016/j.jallcom.2017.05.130>
- [11] M. S. Atas, M. Yildirim, Temporal evolution, coarsening behavior and oxidation resistance of Ni-15Al superalloy, *Journal of Alloys and Compounds* 809 (2019) 151784. <https://doi.org/10.1016/j.jallcom.2019.151784>
- [12] M. S. Atas, M. Yildirim, Morphological development, coarsening, and oxidation behavior of Ni-Al-Nb superalloys, *Journal of Materials Engineering and Performance* 29 (2020) 4421–4434. <https://doi.org/10.1007/s11665-020-04926-3>
- [13] X. Ye, B. Yang, Y. Nie, S. Yu, Y. Li, Influence of Nb addition on the oxidation behavior of novel Ni-base superalloy, *Corrosion Science* 185 (2021) 109436. <https://doi.org/10.1016/j.corsci.2021.109436>
- [14] C. Li, G. Guo, Z. Yuan, W. Xuan, X. Li, Y. Zhong, Z. Ren, Chemical segregation and coarsening of γ' precipitates in Ni-based superalloy during heat treatment in alternating magnetic field, *Journal of Alloys and Compounds* 720 (2017) 272–276. <https://doi.org/10.1016/j.jallcom.2017.05.253>
- [15] S. Tang, L. Ning, T. Xin, Z. Zheng, Coarsening behavior of gamma prime precipitates in a nickel based single crystal superalloy, *Journal of Materials Science & Technology* 32 (2016) 172–176. <https://doi.org/10.1016/j.jmst.2015.10.005>
- [16] G. Wang, H. Ding, R. Chen, J. Guo, H. Fu, Effect of current intensity on microstructure of Ni₃Al intermetallics prepared by directional solidification electromagnetic cold crucible technique, *Acta Metall. Sin.* 53 (2017) 1461–1468. <https://doi.org/10.11900/0412.1961.2017.00099>
- [17] J. Wu, C. Li, Y. Liu, Y. Wu, Q. Guo, H. Li, H. Wang, Effect of annealing treatment on microstructure evolution and creep behavior of a multiphase Ni₃Al-based superalloy, *Materials Science and Engineering A* 743 (2019) 623–635. <https://doi.org/10.1016/j.msea.2018.11.126>
- [18] Y. Wu, Y. Liu, C. Li, X. Xia, J. Wu, H. Li, Coarsening behavior of γ' precipitates in the $\gamma' + \gamma$ area of a Ni₃Al-based alloy, *Journal of Alloys and Compounds* 771 (2019) 526–533. <https://doi.org/10.1016/j.jallcom.2018.08.265>
- [19] L. Tan, Y. Li, W. Deng, Y. Liu, F. Liu, Y. Nie, L. Jiang, Tensile properties of three newly developed Ni-base powder metallurgy superalloys, *Journal of Alloys and Compounds* 804 (2019) 322–330. <https://doi.org/10.1016/j.jallcom.2019.07.002>
- [20] J. Chen, P. Rogers, J. Little, Oxidation behavior of several chromia-forming commercial nickel-base superalloys, *Oxidation of Metals* 47 (1997) 381–410. <https://doi.org/10.1007/BF02134783>
- [21] L. Li, X. Gong, X. Ye, J. Teng, Y. Nie, Y. Li, Q. Lei, Influence of building direction on the oxidation behavior of Inconel 718 alloy fabricated by additive manufacture of electron beam melting, *Materials* 11 (2018) 2549. <https://doi.org/10.3390/ma11122549>
- [22] B. Yu, Y. Li, Y. Nie, H. Mei, High temperature oxidation behavior of a novel cobalt-nickel-base superalloy, *Journal of Alloys and Compounds* 765 (2018) 1148–1157. <https://doi.org/10.1016/j.jallcom.2018.06.275>
- [23] F. Khalid, N. Hussain, K. Shahid, Microstructure and morphology of high temperature oxidation in superalloys, *Materials Science and Engineering A* 265 (1999) 87–94. [https://doi.org/10.1016/S0921-5093\(98\)01181-2](https://doi.org/10.1016/S0921-5093(98)01181-2)
- [24] J. Huang, H. Fang, X. Fu, F. Huang, H. Wan, Q. Zhang, S. Deng, J. Zu, High-temperature oxidation behavior and mechanism of a new type of wrought Ni-

- Fe-Cr-Al superalloy up to 1300 °C, Oxidation of Metals 53 (2000) 273–287.
<https://doi.org/10.1023/A:1004537119922>
- [25] F. Pettit, G. Meier, M. Gell, C. Kartovich, R. Bricknel, W. Kent, J. Radovich, Oxidation and hot corrosion of superalloys, *Superalloys 85* (1984) 651–687.
- [26] P. Berthod, Kinetics of high temperature oxidation and chromia volatilization for a binary Ni-Cr alloy, *Oxidation of Metals* 64 (2005) 235–252.
<https://doi.org/10.1007/s11085-005-6562-8>
- [27] M. Li, X. Sun, J. Li, Z. Zhang, T. Jin, H. Guan, Z. Hu, Oxidation behavior of a single-crystal Ni-base superalloy in air. I: at 800 and 900 °C, *Oxidation of Metals* 59 (2003) 591–605.
<https://doi.org/10.1023/A:1023604214245>
- [28] C. Tedmon Jr., The effect of oxide volatilization on the oxidation kinetics of Cr and Fe-Cr alloys, *Journal of the Electrochemical Society* 113 (1966) 766.
<https://doi.org/10.1149/1.2424115>
- [29] C. T. Sims, N. S. Stoloff, W. C. Hagel, *Superalloys II*, Wiley, New York 1987. ISBN: 978-0-471-01147-7.
- [30] X. Li, S. He, X. Zhou, Y. Zou, Z. Li, A. Li, X. Yu, Effects of rare earth yttrium on microstructure and properties of Ni-16Mo-7Cr-4Fe nickel-based superalloy, *Materials Characterization* 95 (2014) 171–179.
<https://doi.org/10.1016/j.matchar.2014.06.016>
- [31] M. Kutz, *Handbook of Environmental Degradation of Materials*, William Andrew 2018.
<https://doi.org/10.1016/C2016-0-02081-8>
- [32] F. Weng, H. Yu, C. Chen, K. Wan, High-temperature oxidation behavior of Ni-based superalloys with Nb and Y and the interface characteristics of oxidation scales, *Surface and Interface Analysis* 47 (2015) 362–370. <https://doi.org/10.1002/sia.5718>
- [33] B. A. Pint, Optimization of reactive-element additions to improve oxidation performance of alumina-forming alloys, *Journal of the American Ceramic Society* 86 (2003) 686–95.
<https://doi.org/10.1111/j.1151-2916.2003.tb03358.x>
- [34] B. A. Pint, Experimental observations in support of the dynamic-segregation theory to explain the reactive-element effect, *Oxidation of Metals* 45 (1996) 1–37. <https://doi.org/10.1007/BF01046818>
- [35] D. Naumenko, B. A. Pint, W. Quadackers, Current thoughts on reactive element effects in alumina-forming systems: In memory of John Stringer, *Oxidation of Metals* 86 (2016) 1–43.
<https://doi.org/10.1007/s11085-016-9625-0>
- [36] F. Stott, G. Wood, J. Fountain, The influence of yttrium additions on the oxidation resistance of a directionally solidified Ni-Al-Cr₃C₂ eutectic alloy, *Oxidation of Metals* 14 (1980) 135–146.
<https://doi.org/10.1007/BF00603990>
- [37] Y. Zhang, D. Zhu, D. A. Shores, Effect of yttrium on the oxidation behavior of cast Ni-30Cr alloy, *Acta Metallurgica et Materialia* 43 (1995) 4015–4025.
[https://doi.org/10.1016/0956-7151\(95\)00093-B](https://doi.org/10.1016/0956-7151(95)00093-B)
- [38] Y. Ping, W. Wen, W. Fuhui, Influence of cyclic frequency on oxidation behavior of K38 superalloy with yttrium additions at 1273 K, *Journal of Rare Earths* 29 (2011) 119–123.
[https://doi.org/10.1016/S1002-0721\(10\)60415-2](https://doi.org/10.1016/S1002-0721(10)60415-2)
- [39] B. Beaudry, A. Daane, Yttrium-nickel system, *Trans. Met. Soc. AIME* 218 (1960).
- [40] C. K. Sudbrack, Decomposition behavior in model Ni-Al-Cr-X superalloys: Temporal evolution and compositional pathways on a nanoscale, Northwestern University Evanston, IL, 2004.
- [41] J. M. Song, K. L. Lin, Behavior of intermetallics in liquid Sn-Zn-Ag solder alloys, *Journal of Materials Research* 18 (2003) 2060–2067.
<https://doi.org/10.1557/JMR.2003.0290>
- [42] M. H. Mahdavi, M. F. Mohd Sabri, S. Mohd Said, I. A. Badruddin, S. Rozali, Effect of aging on mechanical properties of Sn-Cu-Fe-Bi solder alloy, *Solid State Science and Technology* 26 (2018) 70–77.
- [43] J. Li, X. Li, L. Liu, S. Lu, Mechanism of anomalous eutectic formation in the solidification of undercooled Ni-Sn eutectic alloy, *Journal of Materials Research* 23 (2008) 2139–2148.
<https://doi.org/10.1557/JMR.2008.0259>
- [44] C. Booth-Morrison, R. D. Noebe, D. N. Seidman, Effects of tantalum on the temporal evolution of a model Ni-Al-Cr superalloy during phase decomposition, *Acta Materialia* 57 (2009) 909–920.
<https://doi.org/10.1016/j.actamat.2008.10.029>
- [45] P. J. Bocchini, C. K. Sudbrack, R. D. Noebe, D. C. Dunand, D. N. Seidman, Effects of titanium substitutions for aluminum and tungsten in Co-10Ni-9Al-9W (at.%) superalloys, *Materials Science and Engineering A* 705 (2017) 122–132.
<https://doi.org/10.1016/j.msea.2017.08.034>
- [46] E. Y. Plotnikov, Z. Mao, S.-I. Baik, M. Yildirim, Y. Li, D. Cecchetti, R. D. Noebe, G. Martin, D. N. Seidman, A correlative four-dimensional study of phase-separation at the subnanoscale to nanoscale of a NiAl alloy, *Acta Materialia* 171 (2019) 306–333.
<https://doi.org/10.1016/j.actamat.2019.03.016>
- [47] Y. Wu, Y. Li, Y. Xu, M. Kang, J. Wang, B. Sun, Unveiling the mechanism of yttrium-related microstructure inhibiting or promoting high-temperature oxidation based on Ni-Al-Y alloys, *Acta Materialia* 211 (2021) 116879.
<https://doi.org/10.1016/j.actamat.2021.116879>
- [48] Y. Wu, Y. Li, Y. Xu, M. Kang, J. Wang, B. Sun, Unveiling the precipitation-induced high-temperature oxidation behavior in a Ni-Al-Y alloy, *Materials Letters* 297 (2021) 129977.
<https://doi.org/10.1016/j.matlet.2021.129977>
- [49] A. S. Khanna, High Temperature Oxidation, *Handbook of Environmental Degradation of Materials*, Elsevier 2005, pp. 105–152.
<https://doi.org/10.1016/B978-081551500-5.50008-2>